Nano Energy 36 (2017) 303–312

Contents lists available at ScienceDirect

Nano Energy

journal homepage: www.elsevier.com/locate/nanoen

Full paper

Insight into interfaces and junction of polycrystalline silicon solar cells by kelvin probe force microscopy

Yong-Ji Chen[1], Ming-Jian Zhang[1], Sheng Yuan, Yang Qiu, Xing-Bo Wang, Xing Jiang, Zhou Gao, Yuan Lin, Feng Pan*

School of Advanced Materials, Peking University Shenzhen Graduate School, Shenzhen 518055, China

ARTICLE INFO

Keywords:
KPFM
Solar cell
Interfaces
p-n junction

ABSTRACT

Kelvin probe force microscopy (KPFM) is a powerful tool to measure surface potential with resolutions in the order of atomic/nanometer scales, and could also provide direct measurements of the surface potential on interfaces and junctions of solar cell devices. In this paper, the whole surface potential distribution along the cross-section of the polycrystalline silicon solar cell was illustrated by KPFM for the first time. Interestingly, the surface potential presents a two-stepwise downward profile from Al electrode to Ag electrode, and surface potential skip-steps occur at Al/p-Si interface and p-n junction, respectively. Notably, the p^+ layer due to the Al doping was firstly identified by KPFM. Devices of three different efficiencies are tested and showed that the skip-step value at Ag/Si interface is linearly correlated with the device efficiency. So the surface potential skip-step value at Ag/Si interface is proposed to be an important parameter to evaluate the quality of Ag/Si interface. By combination of SEM, TEM and KPFM characterizations with performance measurement of the solar cells, we get deep insight relationships of compositions and morphologies around metal/semiconductor interfaces and junction in the atomic and nanometer scales, and find correlations between these structures and electrical/photoelectrical properties of devices. These studies are helpful to understand the device physical properties and provide potential routes to improve device efficiency.

1. Introduction

Polycrystalline silicon solar cells take a great market share due to its high efficiency, long-term stability and low cost. Although the power conversion efficiency of polycrystalline silicon solar cell has exceed to 18%, there are few directly tools to research the interfaces and the operating principle of solar cell. It is well known that the quality and properties of the interfaces between different layers is the key part to determine the device performance in all heterojunction-based devices [1–3]. There exist three interfaces or junction of Ag-/n-Si, n-Si/p-Si and p-Si/Al in a classical device structure (Ag/n-Si/p-Si/Al) of polycrystalline silicon solar cell, which are the core structures to determine the device efficiency. So it is very important to get insight into relationship between these interfaces and junction and performance of polycrystalline silicon solar-cells by creating novel measurement methods with resolutions in the order of atomic and nano-scales versus electrical or photo-electrical properties, which will be helpful to control the quality of these interfaces for obtaining high-efficiency devices. Many efforts have been devoted to observe the morphology of these interfaces by scanning electron microscopy (SEM) and transmission electron microscopy (TEM). In comparison, there still lack appropriate tools to measure the electrical properties of these interfaces, including junction location, depth, and electrical potential distribution in the whole devices.

One kind of functions in atomic force microscopy (AFM) is Kelvin probe force microscopy (KPFM), which is also known as surface potential microscopy. Since its first introduction by Nonnenmacher et al. in 1991 [4], KPFM has been used extensively as a unique method to characterize the atomic and nano-scale electronic or electrical properties of metal/semiconductor surfaces and semiconductor devices. Recently, KPFM has been demonstrated as a powerful tool for surface potential measurements, due to of its atomic-level spatial resolution [5–10].

The surface potential relates to many surface phenomena, including catalytic activity, reconstruction of surfaces, doping and band-bending of semiconductors, charge trapping in dielectrics and corrosion [11–14]. Combining TEM, SEM and KPFM characterizations, we can get the mapping of composition and surface potential to give information

* Corresponding author.
E-mail address: panfeng@pkusz.edu.cn (F. Pan).
[1] Yong-Ji Chen and Ming-Jian Zhang contributed equally to this work.

http://dx.doi.org/10.1016/j.nanoen.2017.04.045
Received 15 December 2016; Received in revised form 18 April 2017; Accepted 21 April 2017
Available online 22 April 2017

about the distribution of electron of the local structures on the surface of polycrystalline silicon solar cells [15–20]. It will be very helpful to observe the surface potential distribution at atomic or nano scales for the device evaluation and design.

In this paper, the whole surface potential distribution along the cross-sections of the polycrystalline silicon solar cell was illustrated by KPFM for the first time. Moreover, by combination of TEM, SEM and KPFM characterization with performance measurement of polycrystalline silicon solar cells, three devices with different efficiencies were tested and showed that there existed a linear correlation between the surface potential distribution and the device efficiency. These studies are helpful to understand the device physical properties and provide potential routes to improve solar cell efficiency [21–23].

2. Experimental section

2.1. Device fabrication

Polycrystalline silicon solar cell devices used in this research are prepared by screen-printing DuPont PV18H silver paste on the commercial semi-finished devices with a SiN_x/n-Si/p-Si/Al configuration and subsequently performing calcination in a seven-section meshbelt furnace. The semi-finished devices were bought from Tian-Si New Energy Company. The seven-section meshbelt furnace was designed by ourselves and assembled by Hefei Ke-Jing Materials Technology Company.

2.2. Device characterization

The current density versus voltage (J–V) characteristic curves of the devices are recorded using a Keithley 2602A sourcemeter (Keithley Instruments Inc., Cleveland, OH, USA) under one sun, AM 1.5G irradiation (100 mW/cm^2) from a solar simulator (Abet Technologies Model 11000A Sun 3000 Solar Simulator). The illumination intensity is calibrated using a standard single crystal silicon solar cell. All of the measurements are performed under ambient atmosphere at room temperature (25 °C).

2.3. Device cross-section preparation

The cross-section samples of polycrystalline silicon solar cell are processed by an Ar^+ Ion Beam Milling System (Leica EM TIC 3X, Leica Inc). First, a cleaved polycrystalline silicon solar cell (12 mm×3 mm, cut by laser cutting machine) is loaded into the high vacuum chamber. Then it is milled by three Ar^+ ion beams using beam voltage of 7.5 kV and beam current of 2.8 mA for 3.5 h and then polishing with voltage of 4.5 kV and beam current of 1.6 mA for 1.5 h. (Fig. 1a). A fresh and smooth cross-section of polycrystalline silicon solar cell can be achieved. And the surface potential along the cross-section was directly measured by KPFM (Fig. 1b).

2.4. Device cross-section characterization

The morphology of the cross-sections for polycrystalline silicon solar devices are characterized using SEM (SEM, ZEISS Supra 55-VP). The interface of Ag/glass/Si of the samples were analyzed by transmission electron microscope (TEM, FEI Tecnai G2 F30). And energy dispersive X-ray spectroscopy (EDX) was employed to analyze the surface element distribution and composition of samples. The sample of the interface of Ag/glass/Si for TEM was prepared by Focused Ion Beam (FIB, FEI, Scios) followed by Ion Beam Modulating (Fig. S3). Firstly, a relatively flat region was selected, then Pt was deposited on the surface of selected section for protecting the interface with a thickness of Pt deposited up to 1 μm. A Ga ion beam (30 kV, 1 nA) was employed to cut all selected areas. Then the cut cross-sectional sample was transferred to a special Company "U" style copper network for further ion milling. A final sample suitable for TEM with a thickness of ~20 nm or so was obtained by ion milling repeated with different Ga ion beam followed by (30 kV, 50 pA), (20 kV, 50 pA), (10 kV, 30 pA), (5 kV, 16 pA) and (2 kV, 8 pA). The KPFM surface potential measurements of device cross-sections are carried out by a MultiMode 8-HR AFM (Bruker Corporation, Germany) using Pt/Ir-coated conducting tips (SCM-PIT) with a resonance frequency of 75 kHz and a spring constant of 2.8 N/m. A two-pass scan amplitude modulated KPFM (AM-KPFM) is used to measure the surface potential in a glove box (H_2O < 1 ppm, O_2 < 1 ppm). During the first pass, standard alternating current (AC) mode imaging (typical tip oscillation amplitude 20 nm) is performed to acquire the topography and phase signal of the sample; in the second pass, the tip is lifted up by a certain height (typically 80 nm) and scanned on the basis of the topography line obtained from the first pass. An AC voltage is applied to actuate the cantilever, and the direct current (DC) voltage applied to the tip that nullifies the tip–sample interaction is collected as the SP signal. The device-wiring configuration during cross-section characterization is shown in Fig. 1b. Ag electrode is grounded when scanning Part I (Ag/n-Si/p-Si), and Al electrode is grounded when scanning Part II (Al/p-Si).

3. Results and discussions

We have prepared three polycrystalline silicon solar cell devices with different power conversion efficiencies (PCE=8.81%, 13.25% and 15.27%) by adopting different calcination conditions. Three kinds of calcination conditions are presented in Fig. S1. It is easy to find that the main difference between these three conditions is the annealing time at the highest temperature. The longest annealing time led to a lowest efficiency (8.81%), and the highest efficiency (15.27%) was originated from the moderate annealing time. J–V curves are presented in Fig. 1c, and the corresponding photovoltaic parameters are listed in Table S1. As shown in Fig. S2, the efficiency was positively correlated with short-circuit current density (J_{sc}) and fill factor (FF), which are significantly

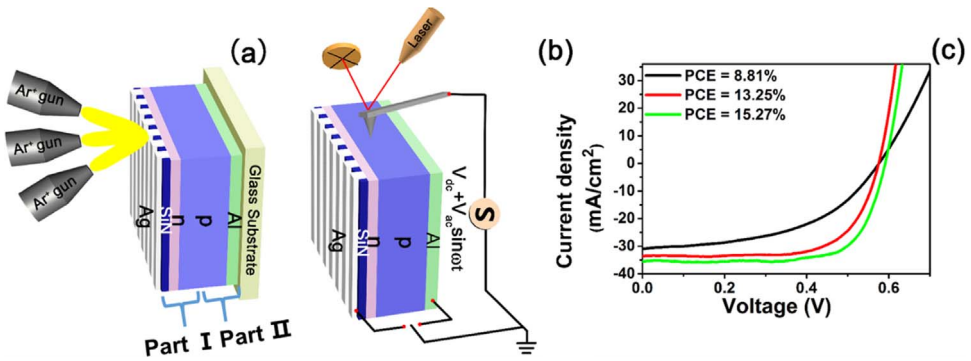

Fig. 1. (a) Schematic illustration of Ar^+-beam milling configuration to expose a smooth cross-section of polycrystalline silicon solar cell device; (b) Schematic illustration of the surface potential measurement by KPFM along the cross-section; (c) J–V curves of polycrystalline silicon solar cell devices under standard test condition (AM 1.5G illumination, 100 mW/cm^2, 25 °C).

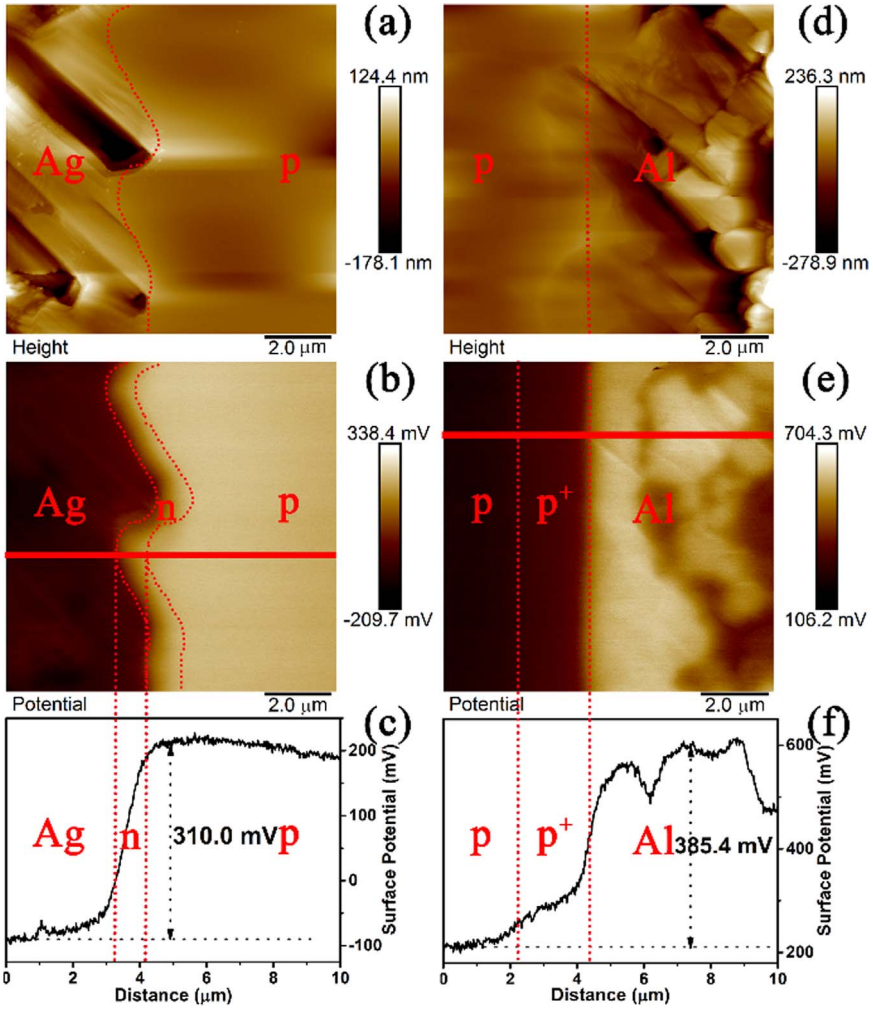

Fig. 2. (a) and (d) are topography images of Part I and Part II, respectively;(b) and (e) are surface potential images of Part I and Part II, respectively; (c) and (f) are surface potential line profiles (corresponding to solid red lines) of Part I and Part II, respectively.

affected by different calcination conditions.

The total cross-sectional thickness of the device is about 180 μm. Owing to the limited detect region (about 100 μm ×100 μm) of KPFM, it is impossible to measure the whole cross-section in one scan. Because of the small thickness of n-Si layer, the interfaces of Ag/n-Si and n-Si/p-Si are located very closely. So we divided the whole cross-section into two parts, Part I (Ag/n-Si/p-Si) and Part II (Al/p-Si) for convenience (shown in Fig. 1a). To scan Part I, we grounded Ag electrode and then scan from Ag electrode to n-Si layer and then to p-Si layer. To scan Part II, Al electrode was grounded and then scanned from Al electrode to p-Si layer.

First , the difference value of surface potential of Part I and Part II have been gotten by KPFM under dark condition. Taking the device with the highest power conversion efficiency (15.27%) as a representative, we respectively measured the topography image and the surface potential image of the cross-section (Fig. 2). We can clearly distinguish Ag-layer, Si-layer and Al-layer from Fig. 2a and d. But, it is very difficult to distinguish n-Si and p-Si layers or p-Si and p^+ layers by the morphology image, because n-Si layer is obtained by the thermal diffusion of P element into the p-Si layer and p^+ layer is formed due to the doping of Al into the p-Si layer in the calcination process.

Correspondingly, the surface potential images for two parts are presented in Fig. 2b and e below. The dark region on the left is Ag-layer, the khaki region on the right is p-Si layer and the middle region colored in light brown is n-Si layer in Fig. 2b. As shown in Fig. 2e, the dark region on the left is p-Si layer, the khaki region on the right is p-Si layer and the middle region colored in dark red is p^+ layer. In order to further analyze the surface potential variation along the cross-section, the red line profiles perpendicular to the Ag/n-Si/p-Si and p-Si/Al interfaces were extracted and illustrated in Fig. 2c and f. It is clear that a potential skip-step of about 310 mV appeared in Part I. Viewing along the red dotted line, we could find that this skip-step is mainly located in the n-Si region. On the other side, as shown in Fig. 2f, it presented two skip-steps, one is gentle and the other is sharp. The gentle one corresponds to the p^+ region with about 100 mV and the sharp one with about 280 mV corresponds to the Al/Si interface.

Based on the analysis above, we could combine these two parts and obtain an integrated surface potential profile along the whole cross-section. As shown in Fig. 3, it is clear that two big skip-steps occurred from the Al electrode to the Ag electrode. One is located in Ag/n-Si/p-Si interface, and the other is located at the Al/p-Si interface. As we all know, there is a p–n junction in polycrystalline silicon solar cell, which is created by P elemental doping into p-type silicon. The p-type silicon region contains excessive holes, while the n-type region contains excessive electrons. Because the density difference of different carriers, electrons from n-type silicon region at the p–n interface tend to diffuse into p-type silicon region, leaving behind positive charges in n-type silicon region. Likewise, holes from p-type silicon region at the p–n interface tend to diffuse into n-type silicon region, leaving behind negative charges in p-type silicon region. So, a built-in potential is formed at the p–n interface. And the real built-in potential is approximately equal to open-circuit voltage of solar cell. In our paper,

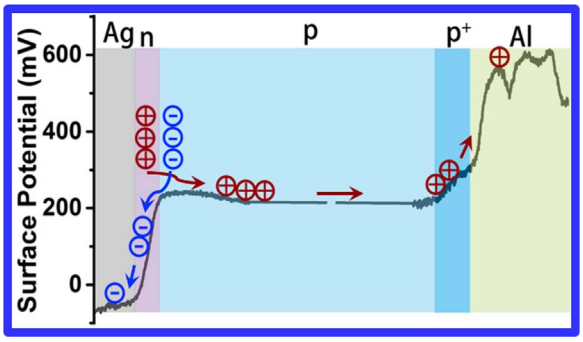

Fig. 3. The whole surface potential distribution along the cross-section.

the open-circuit voltage of cell 1–3 are 576 mV, 575 mV, 591 mV, respectively, in Table S1. Under the action of built-in potential, electrons are pushed to n-type silicon layer and transferred to Ag electrode. And holes are pushed to p-type silicon layer (Fig. 3). And there is a p^+ layer between p-Si layer and Al electrode. Because of p^+ layer has more holes than p silicon layer. So there is a hole density gradient from bulk p-type silicon region to p/p^+ interface. This hole density gradient drives the holes in bulk p-type silicon region to move to the p^+ layer, then transferred to Al electrode. In conclusion, just because of the action of built-in potential and hole density gradient lead to the electrons and holes in solar cells redistribution. So result in the surface potential change from Ag electrode to Al electrode as Fig. 3. It seem that there is a potential between Ag electrode and Al electrode of solar cell.

In Fig. 3, we also could trace out the transport routine of photo-generated carriers in the whole photovoltaic process as follows. When the device is exposed to the light, the photo-generated carriers are firstly produced in the p/n junction region. Then forced by built-in potential. The electrons are collected by Ag electrode, and the holes are transferred to the p-Si/Al interface. On the whole, this surface potential profile with two skip-steps is the results of electrons and holes redistribution. It could be predicted that the values of the skip-steps are correlated with the quality of Ag/Si interface and Al/Si interface.

In order to validate the conjecture, the surface potential measurement was performed on three devices with increasing photoelectric conversion efficiencies (PCE=8.81%, 13.25%, 15.27%). The topography images, surface potential images and the corresponding line profiles of Part I and Part II for three devices tested under dark are shown in Figs. 4 and 5, respectively.

At first, the topography images of Part I, II for three devices are presented in Fig. 4a, d, g and Fig. 5a, d, g. Obviously, it's easy to figure out Ag-layer, p-Si layer and Al-layer, but it's also difficult to find out n-Si and p^+ layers from the topography images. And the corresponding

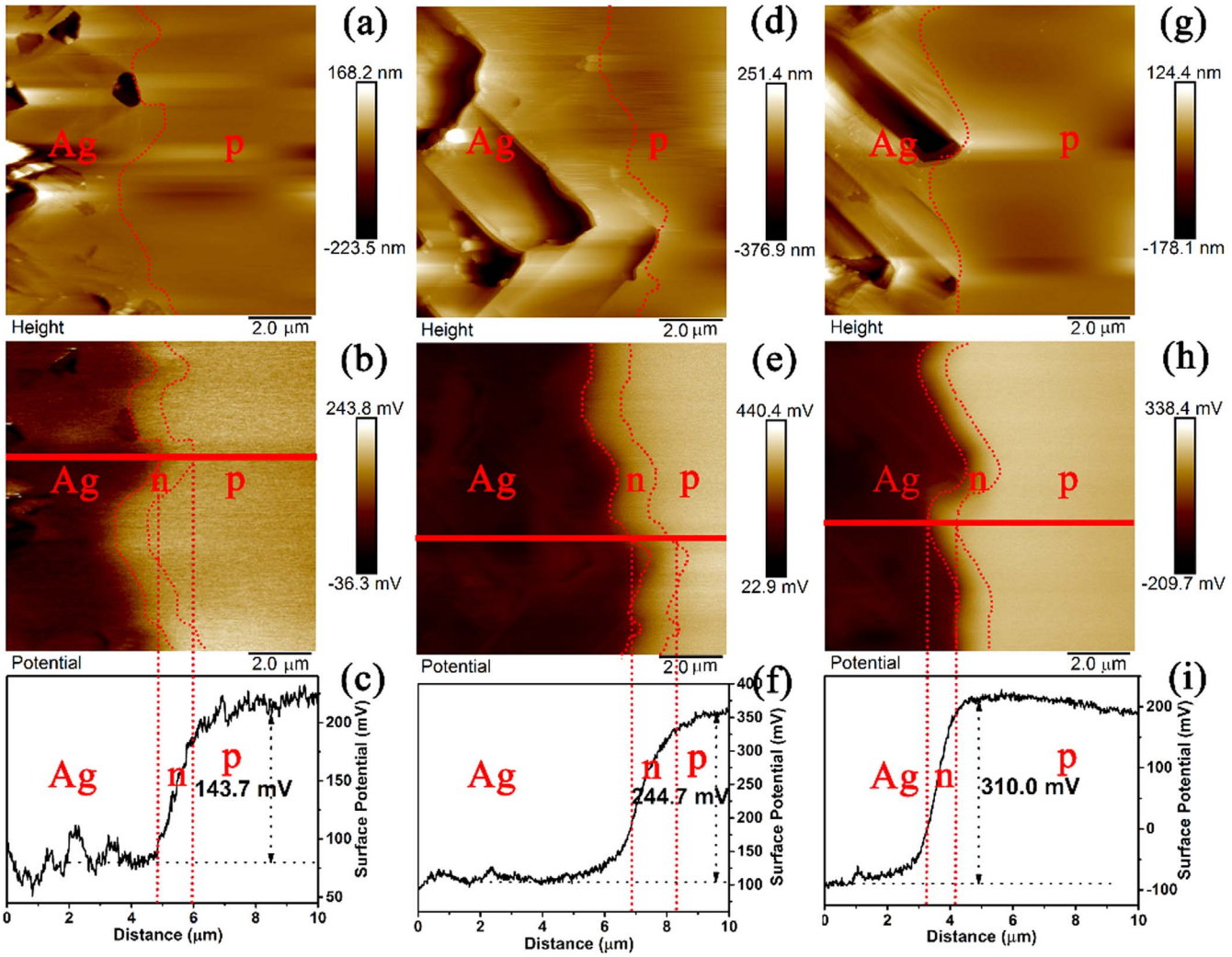

Fig. 4. Topography, surface potential images and surface potential line profiles of Part I for polycrystalline silicon solar cell devices with different efficiencies by KPFM under dark condition. (a), (b) and (c) are topography, surface potential image and line profile for the device with conversion efficiency of 8.81%, respectively; (d), (e) and (f) are topography, surface potential image and line profile for the device with conversion efficiency of 13.25%, respectively; (g), (h) and (i) are topography, surface potential image and line profile for the device with conversion efficiency of 15.27%, respectively.

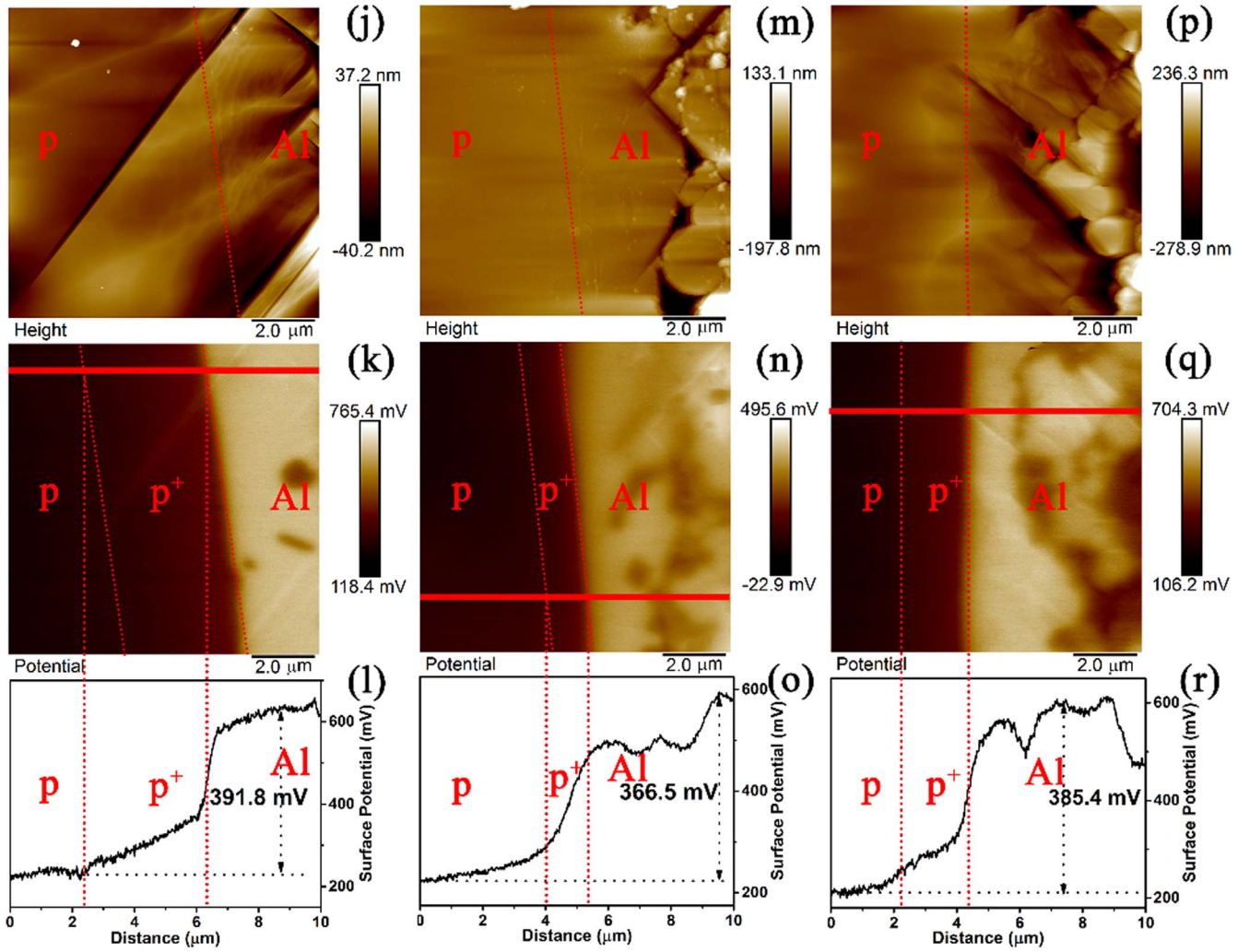

Fig. 5. Topography, surface potential images and surface potential line profiles of Part II for polycrystalline silicon solar cell devices with different efficiencies by KPFM under dark condition. (a), (b) and (c) are topography, surface potential image and line profile for the device with conversion efficiency of 8.81%, respectively; (d), (e) and (f) are topography, surface potential image and line profile for the device with conversion efficiency of 13.25%, respectively; (g), (h) and (i) are topography, surface potential image and line profile for the device with conversion efficiency of 15.27%, respectively.

surface potential images from Ag-layer to p-layer are recorded in Fig. 4b, e and h. The middle n-Si layers could be identified in these three images due to the color contrast. Owing to the differences of probes, the absolute values of surface potentials for p-Si and Ag electrode are insignificant, but the relative value can reflect the case of Ag/Si interface. And the corresponding line profiles are shown in Fig. 4c, f and i for three devices. The skip-step values are 144, 244 and 310 mV, respectively.

Similarly, the p^+ layer which between p-Si layer and Al electrode in dark red color is found in Fig. 5b, e and h. There also are two skip-steps and the total skip-step values for three devices are shown in Fig. 5c, f and i. They are 392, 366 and 385 mV, respectively. They are very close which indicate that the surface potential skip-step value of p/Al interface is basically not related with power conversion efficiency of solar cells.

In order to further study and compare with the results under dark condition, we have tested the same samples under illumination condition (AM 1.5G illumination, 100 mW/cm2, 25 °C) by KPFM with the same experimental procedure. Just as expected, it has the similar tendency as that under dark condition.

As shown in Fig. 6, the skip-step values of Part I are 281.9, 416.8 and 530.6 mV, respectively. And the skip-step values of Part II are 503.3, 507.1 and 514.8 mV, respectively, in Fig. 7. The skip-step values for both Part I and Part II are larger than the values under dark condition. This might be caused by the photoelectric response of p-n junction under illumination. Photo-generated carriers arise under light, then are transferred and gather to the electrodes under built-in potential. This would lead to the increasing of carrier densities on the both electrodes than that under dark condition, resulting in the larger potential skip-step values.

As shown in Fig. 8, we have found that a positive correlation between the potential skip-steps of Ag/n/p layers and photoelectric conversion efficiency (PCE). But the potential skip-steps of Al/p layers keep basically constant with the photoelectric conversion efficiency. Due to the formation of continuous Al-Si alloy layer, an excellent electric contact was formed between Al electrode and Si layer. So, there is a good contact of Al/Si interface with a very tiny contact resistance. In contrast, there is a glass layer between Ag electrode and n-type silicon layer. The quality of this glass layer greatly depends on the calcination condition of solar cell, and lead to the variable contact resistance. As we know, the value of contact resistance has a great influence on power conversion efficiency of solar cell. So, we have measured the contact resistance of Ag/Si interface by the transmission line model (TLM) method to evaluate the calcination quality of glass layer [24–27]. The test result as shown in Table S1 and Fig. 9f, the lower contact resistance of Ag/Si interface accompanies with the higher power conversion efficiency. So we could deduce that the contact resistance has a great impact on the skip-step value at the Ag/Si

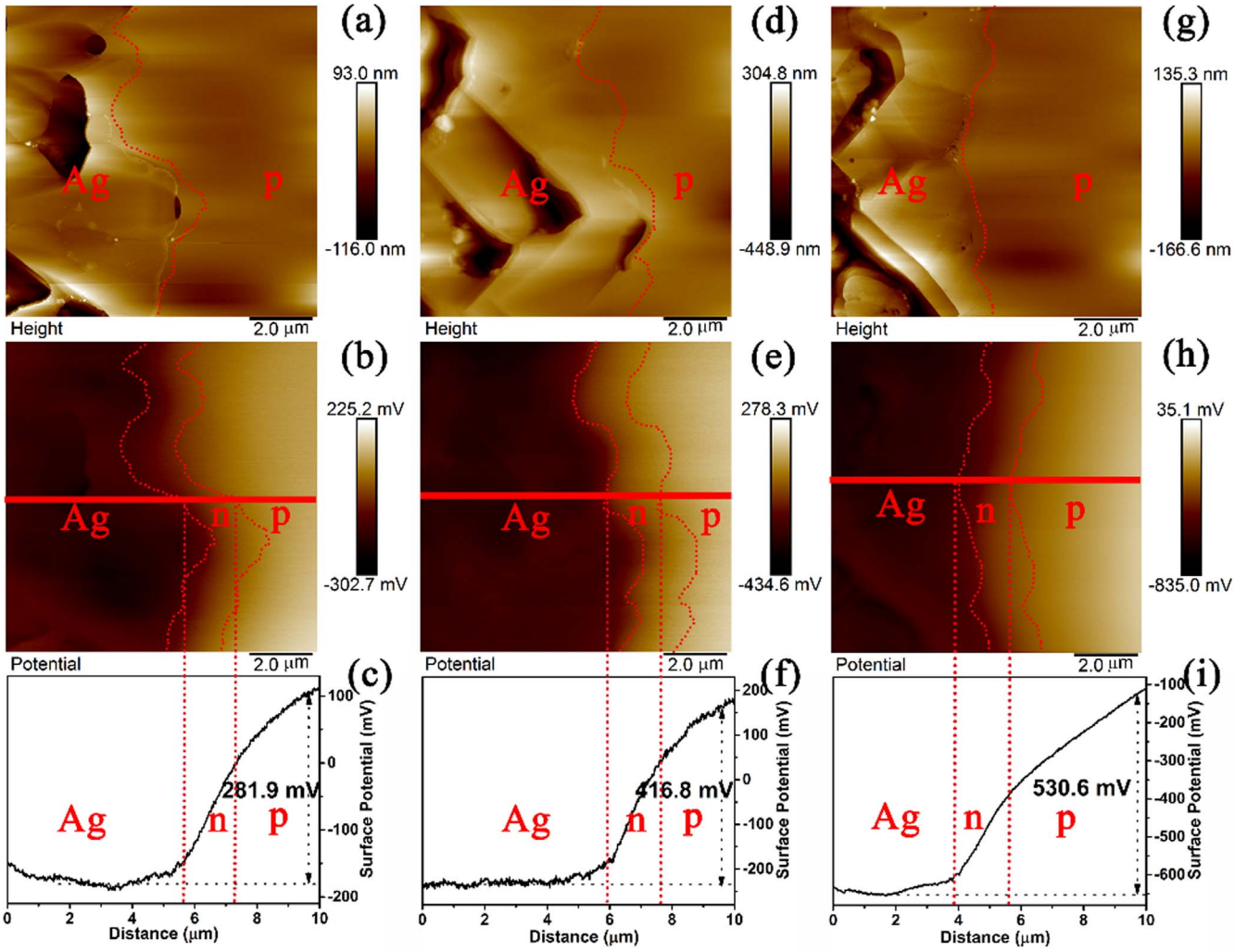

Fig. 6. Topography, surface potential images and surface potential line profiles of Part I for polycrystalline silicon solar cell devices with different efficiencies by KPFM under light condition (AM 1.5G illumination, 100 mW/cm^2, 25 °C). (a), (b) and (c) are topography, surface potential image and line profile for the device with conversion efficiency of 8.81%, respectively; (d), (e) and (f) are topography, surface potential image and line profile for the device with conversion efficiency of 13.25%, respectively; (g), (h) and (i) are topography, surface potential image and line profile for the device with conversion efficiency of 15.27%, respectively.

interface. And the increasing of contact resistance at Ag/Si interface will raise the potential barrier for electrons transfer to the Ag/Si interface. The results of TEM, SEM and EDS images further illustrate the features around the Ag/Si interface shown in Fig. 9a, b, c, d and Fig. 10a, from which Ag electrode, glass layer and Si-layer can be clearly distinguished. It can be found that the higher density of Ag crystallites in glass layer can increase the electrical conductivity of glass layer and bring with lower contact resistance, finally lead to a higher conversion efficiency of solar cell.

Based on the analysis above, we could conclude that the efficiency was positively correlated with the skip-step value of Ag/Si interface, which is highly sensitive to the calcination condition. The appropriate calcination condition leads to the high-quality Ag/Si interface, characterized with a high surface potential skip-step value. So the potential skip-step value at Ag/ Si interface could be acted as an important parameter to evaluate the quality of Ag/Si interface, and could also assist to choose appropriate calcination condition for high-performance device fabrication.

Dominik Ziegler and Andreas Stemmer have indicated that amplitude modulated KPFM (AM-KPFM) detection is sensitive to long-range electrostatic forces, and the tip's apex, the cone and the cantilever strongly contribute to the KPFM Signal. The resulting lateral averaging can lead to severe errors or even contrast inversion of the recorded surface potentials. The effective surface potential can be restored by deconvolution of the measured Kelvin probe data if the point spread function of the tip is known. And there are various conditions where AM-KPFM detection shows a dependence on experimental parameters such as the strength of the electrical excitation, or the capacitance between tip and sample which results in surface potentials varying with lift-height. Just for reasons as above, they demonstrate that FM detection overcomes such errors to a large extent. Because amplitude modulated KPFM is force sensitive but frequency modulated KPFM (FM-KPFM) is force gradient sensitive. However the force gradient decays faster than the force, so FM-KPFM is much more sensitive than AM-KPFM. And FM-KPFM detection shows much less influence from cone and cantilever. As a consequence higher lateral resolution can be achieved and the local surface potential can be measured directly without the need of complex models or deconvolution techniques [28]. There is another solution for the above problems of AM-KPFM, Wagner et al. have demonstrated a novel feedback controller for high resolution which is more superior than traditional lift-mode FM-KPFM setups. This feedback controller is based on a Kalman filter and direct demodulation of sidebands. And which can maintain robust topography feedback and minimal crosstalk [29].

In this paper, we have taken a series of steps to tackle the problem of measuring errors. We have moved the AFM instruments to a glove

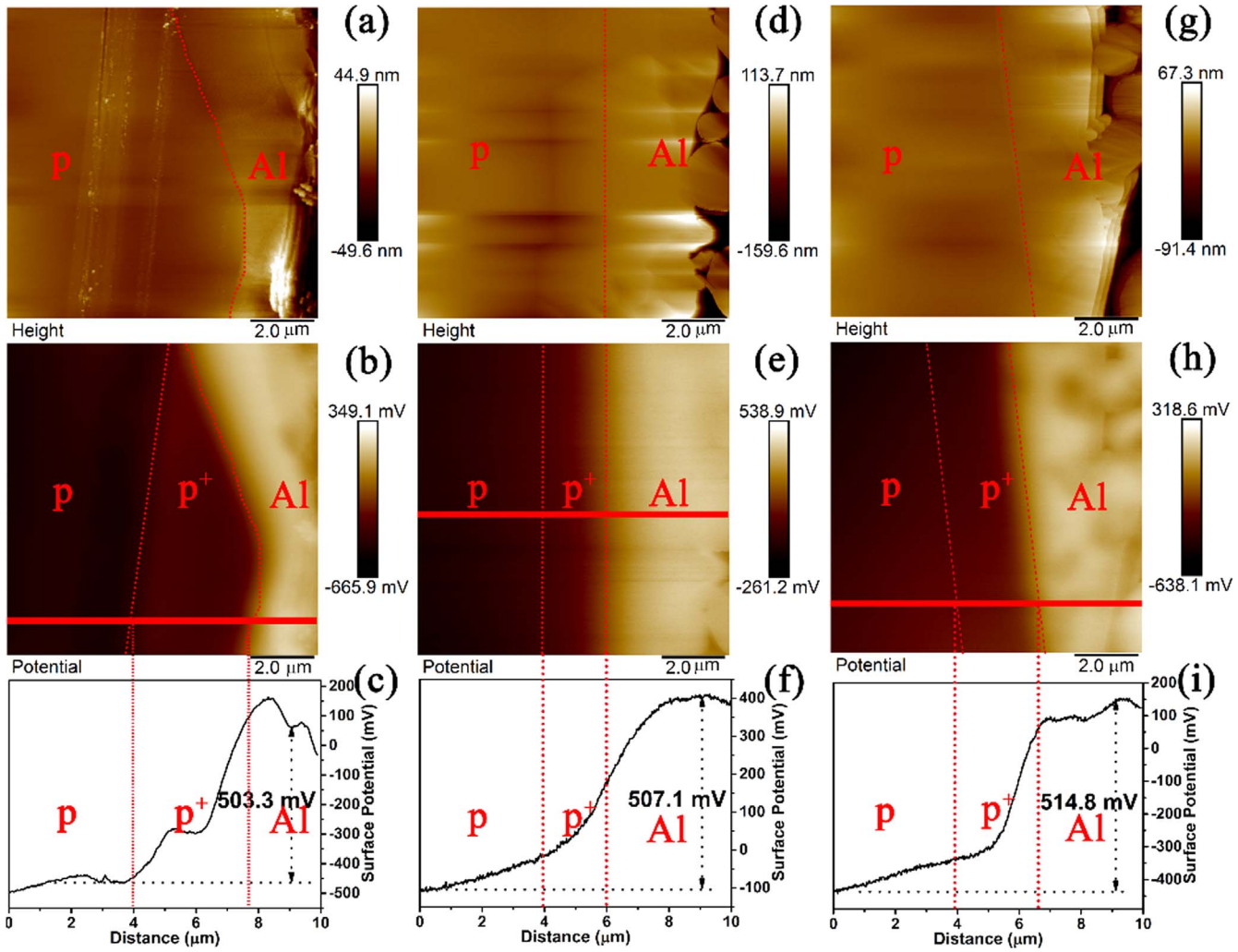

Fig. 7. Topography, surface potential images and surface potential line profiles of Part II for polycrystalline silicon solar cell devices with different efficiencies by KPFM under light condition (AM 1.5G illumination, 100 mW/cm^2, 25 °C). (a), (b) and (c) are topography, surface potential image and line profile for the device with conversion efficiency of 8.81%, respectively; (d), (e) and (f) are topography, surface potential image and line profile for the device with conversion efficiency of 13.25%, respectively; (g), (h) and (i) are topography, surface potential image and line profile for the device with conversion efficiency of 15.27%, respectively.

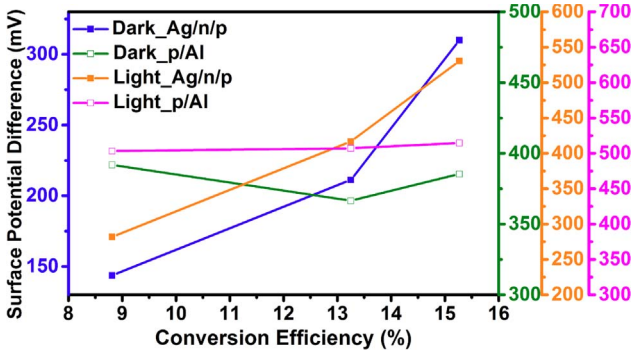

Fig. 8. The change curves of the surface potential skip-step values of Ag/n/p and p/Al with the device efficiency under dark or light condition.

box (Argon atmosphere, H2O < 1 ppm, O2 < 1 ppm) and transfer fresh cross-section of polycrystalline silicon solar cell to glove box immediately to reduce negative influence of surface contamination, oxide layers and potential shielding by the presence of a water film as much as possible. Under the premise of stable operation, we set the lift-height (about 80 nm) as smaller as possible to guarantee the electrostatic force by far exceed van der Waals force for better sensitivity and minimal spatial averaging [30]. And we have got the difference value of surface potential among different layers, which is a relative value that should reduce topography crosstalk to some extent.

4. Conclusions

In summary, the whole surface potential distribution along the cross-section of the polycrystalline silicon solar cell was illustrated by KPFM for the first time. Interestingly, the surface potential presents a two-stepwise downward profile from Al electrode to Ag electrode, and each surface potential skip-step occurs at Al/Si interface and p/n junction, respectively. Notably, the P$^+$ layer due to the Al doping was firstly identified by this method. In addition, the potential skip-step value at Ag/Si interface is found to be linearly correlated with the device efficiency. It could be acted as an important parameter to evaluate the quality of Ag/Si interface. Thus, by combination of SEM, TEM and KPFM characterization with performance measurement of polycrystalline silicon solar cells, we get deep insight of compositions and morphologies around metal/semiconductor interfaces and junction in the atomic and nanometer scales, and find correlations of these structures and electrical/photoelectrical properties of devices. Accordingly, a lot of routes, such as element doping to glass layer, replacement of Ag layer with other materials and other ways to decrease the contact resistance and increase potential skip-step value of Ag/Si interface could be adopted to improve the cell efficiency.

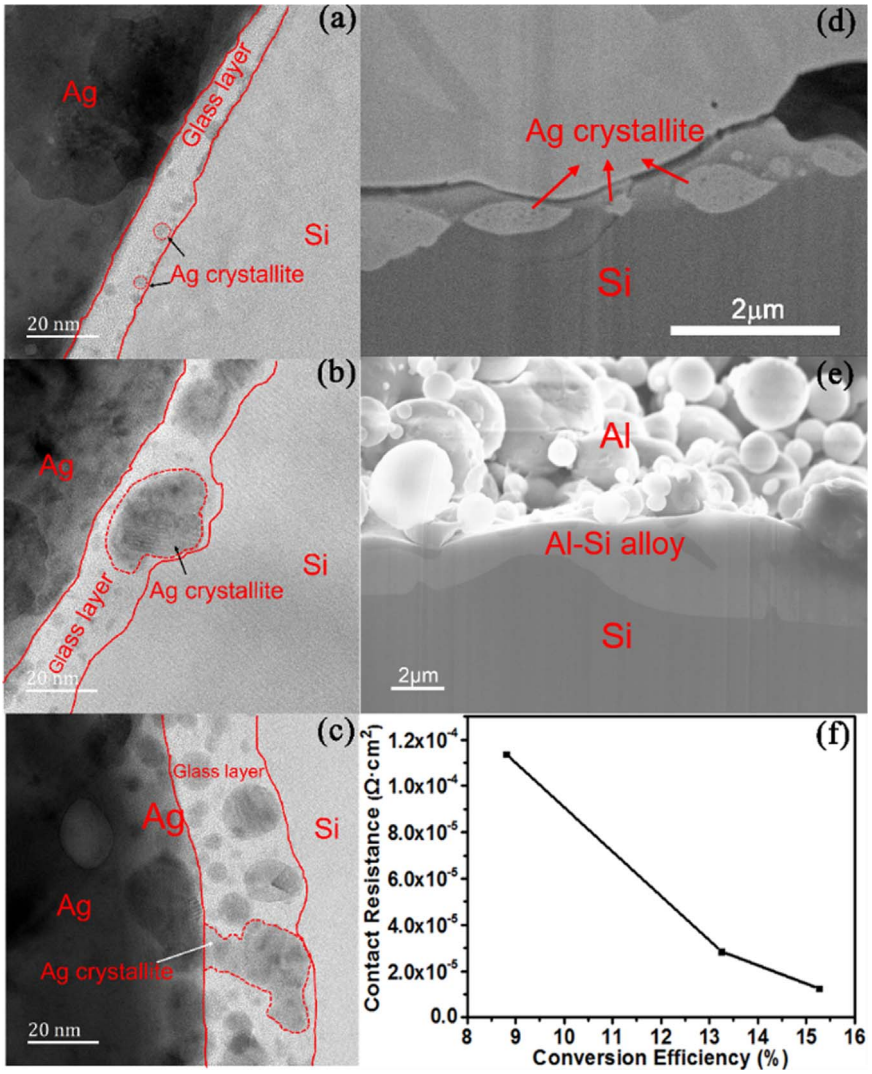

Fig. 9. (a), (b) and (c) are the TEM images of Ag/Si interfaces of polycrystalline silicon solar cell devices with PCE=8.81%, 13.25%, 15.27%, respectively; (d) and (e) are the cross-sectional SEM images for the Ag/Si and Al/Si interfaces of polycrystalline silicon solar cell device with PCE=15.27%, respectively; (f) The changed curve of the contact resistance of Ag/Si interface with the device efficiency.

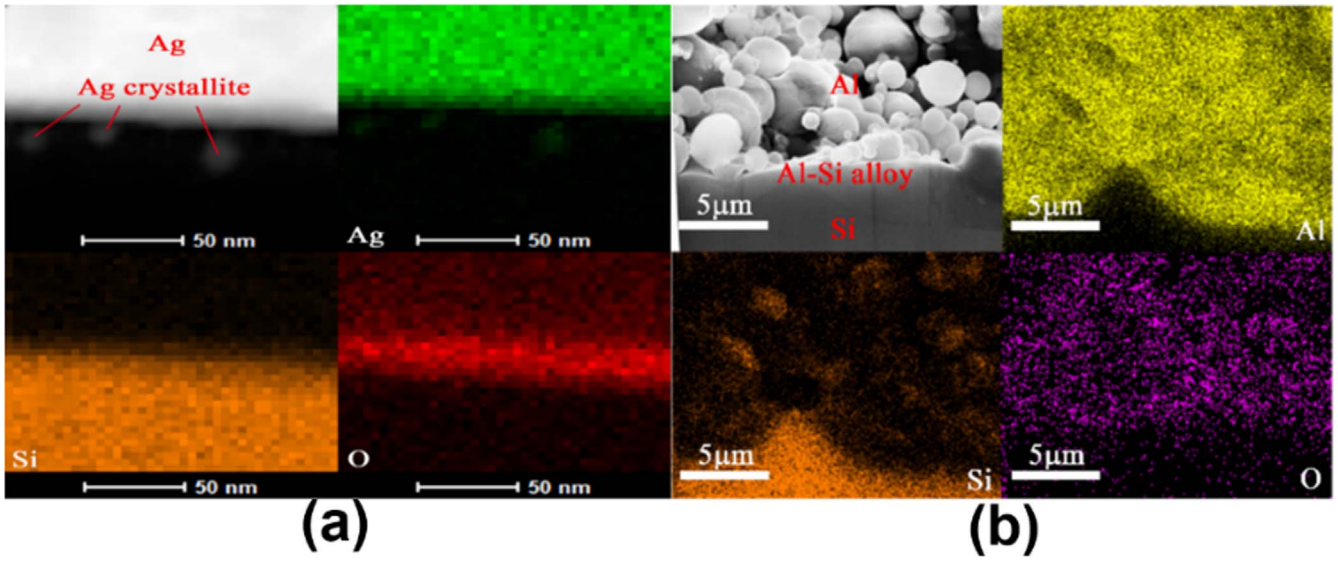

Fig. 10. The cross-sectional EDS mappings of STEM and SEM for the Ag/Si and Al/Si interfaces of cell 3.

Acknowledgements

We thank financial support from the Guangdong Innovative and Entrepreneurial Research Team Program (Grant 2013N080), the Peacock Plan (Grant KYPT20141016105435850), Shenzhen Key Lab (Grant nos. (2012)780 and ZDSY20130331145131323), the International Postdoctoral Exchange Fellowship Program (No. 53 Document of OCPC, 2016). And thank Mr. Shao-Jie Fu for help of sample preparations by FIB and TEM measurements.

Appendix A. Supplementary material

Supplementary data associated with this article can be found in the online version at http://dx.doi.org/10.1016/j.nanoen.2017.04.045.

References

[1] C.H. Lin, S.Y. Tsai, S.P. Hsu, M.H. Hsieh, Sol. Energy Mater. Sol. Cell 92 (2008) 1011–1015.
[2] E. Cabrera, S. Olibet, J. Glatz-Reichenbach, R. Kopecek, D. Reinke, Gunnar Schubert, Energy Procedia 8 (2011) 540–545.
[3] J.D. Fields, M.I. Ahmad, V.L. Pool, J.F. Yu, D.G.V. Campen, P.A. Parilla, M.F. Toney, Nat. Commun. 7 (2016) 11143–11149.
[4] M. Nonnenmacher, M.P. O'Boyle, H.K. Wickramasinghe, Appl. Phys. Lett. 58 (1991) 2921–2923.
[5] W. Melitz, J. Shen, A.C. Kummel, S. Lee, Surf. Sci. Rep. 66 (2011) 1–27.
[6] K.M.F. Shahil, M.Z. Hossain, V. Goyal, A.A. Balandin, J. Appl. Phys. 111 (2012) 1757–1765.
[7] G.L. Hao, X. Qi, L.W. Yang, Y.D. Liu, J. Li, L. Ren, F. Sun, J.X. Zhong, AIP Adv. 111 (2012) 114–122.
[8] M. Zhang, Q. Lin, X. Yang, Z. Mei, J. Liang, Y. Lin, F. Pan, Nano Lett. 16 (2016) 1218–1223.
[9] Q. Lin, Y. Su, M. Zhang, X. Yang, S. Yuan, J. Hu, Y. Lin, J. Liang, F. Pan, Chem. Commun. 52 (2016) 10708–10711.
[10] J. Liang, Q. Lin, H. Li, Y. Su, X. Yang, Z. Wu, J. Zheng, X. Wang, Y. Lin, F. Pan, Appl. Phys. Lett. 107 (2015) 699–753.
[11] Q. Chen, M. Lin, Y. Li, T. Kong, N. Wu, C. Ma, S. Bai, Y. Jin, D. Wu, L. Wei, Nat. Commun. 6 (2015) 7745–7753.
[12] S. Sadewasser, T. Glatzel, Kelvin probe force microscopy, Appl. Phys. Lett. 58 (1991) 2921–2923.
[13] H. Hoppe, T. Glatzel, M. Niggemann, A. Hinsch, M.C. Lux-Steiner, N.S. Sariciftci, Nano Lett. 5 (2005) 269–274.
[14] Th Glatzel, D.F. Marron, Th Schedel-Niedrig, S. Sadewasser, M. Ch Lux-Steiner, Appl. Phys. Lett. 81 (2002) 2017–2019.
[15] A. Kikukawa, S. Hosaka, R. Imura, Appl. Phys. Lett. 66 (1995) 3510–3512.
[16] C.S. Jiang, A. Ptak, B. Yan, H.R. Moutinho, J.V. Li, M.M. Al-Jassim, Ultramicroscopy 109 (2009) 952–957.
[17] F. Robin, H. Jacobs, O. Homan, A. Stemmer, W. Bächtold, Appl. Phys. Lett. 76 (2000) 2907–2909.
[18] A. Liscio, V. Palermo, D. Gentilini, F. Nolde, K. Müllen, P. Samorì, Adv. Funct. Mater. 16 (2006) 1407–1416.
[19] P. Matyba, K. Maturova, M. Kemerink, N.D. Robinson, L. Edman, Nat. Mater. 8 (2009) 672–676.
[20] I. Visoly-Fisher, S.R. Cohen, K. Gartsman, A. Ruzin, D. Cahen, Adv. Funct. Mater. 16 (2006) 649–660.
[21] G.H. Enevoldsen, T. Glatzel, M.C. Christensen, J.V. Lauritsen, F. Besenbacher, Phys. Rev. Lett. 100 (2008) 1151–1156.
[22] C.S. Jiang, H.R. Moutinho, J.F. Geisz, D.J. Friedman, M.M. Al-Jassim, Appl. Phys. Lett. 81 (2002) 2569–2571.
[23] M. Moczała, N. Sosa, A. Topol, T. Gotszalk, Ultramicroscopy 141 (2014) 1–8.
[24] H.H. Berger, J. Electrochem. Soc. 119 (1972) 507–514.
[25] G.K. Reeves, H.B. Harrison, IEEE Electr. Device Lett. 3 (1982) 111–113.
[26] D.K. Schroder, D.L. Meier, IEEE Trans. Electron Dev. 31 (1984) 637–647.
[27] D. Pysch, A. Mette, S.W. Glunz, Sol. Energy Mat. Sol. Cell 91 (2007) 1698–1706.
[28] D. Ziegler, A. Stemmer, Nanotechnology 22 (2011) 4484–4492.
[29] T. Wagner, H. Beyer, P. Reissner, M. Philipp, R. Heike, G. Bernd, S. Andreas, Beilstein J. Nanotechnol. 6 (2015) 2193–2206.
[30] M. Guggisberg, M. Bammerlin, Ch Loppacher, O. Pfeiffer, A. Abdurixit, V. Barwich, R. Bennewitz, A. Baratoff, E. Meyer, H.-J. Güntherodt, Phys. Rev. B 61 (2000) 11151–11158.

Yong-Ji Chen got B.S. from Shihezi University, China, in 2014. He is a master's candidate of the School of Advanced Materials, Peking University, China. He has researched silver pastes of crystalline silicon solar cells since 2014. His main research interests include solar cell and 3D printing materials.

Ming-Jian Zhang got B.S. from College of Chemistry, Nankai University in 2008, Ph.D. from Fujian Institute of Research on the Structure of Matter, Chinese Academy of Sciences (CAS) in 2013. From Jul. 2013 to Sep. 2014, he took the position of assistant research fellow at CAS. From Oct. 2014 to present, he took the position of postdoctor in School of Advanced Materials, Peking University. Ming-Jian Zhang has been engaged in the fields of photoelectrical conversion of solar energy, investigation of electrode materials for Li-ion batteries, crystal growth, structure determination and nonlinear optical (NLO) performance measurement of new chalcogenides.

Sheng Yuan received his Bachelor's degree (BE) from Guizhou University, China, in 2014. He is currently a master student major in materials chemistry in Peking University Shenzhen graduate school. His research is mainly focused on photocatalytic materials and solar cells.

Yang Qiu graduated from Department of mechanical engineering of Tsinghua University, and a present graduate student at the Advanced Materials College in Peking University .The main research direction is the development of equipment for 3D printing technology in the photovoltaic industry and research on the rheological properties for 3D printing silver paste.

Xing Jiang received his B.S. degree in Chemistry from Peking University, China in 2016 and continued his study in Peking University. From 2015 to 2016, he worked on perovskite solar cells as a student in Chun-hui Huang's group. From 2016 to 2017, he worked on silver pastes applied in silicon solar cells as a student in Feng Pan's group. His research interests include preparation and application of solar cells.

Xing-Bo Wang was born in Liaoning, China, in 1993. He received his B.S. from Peking University in 2016 and then entered School of Advanced Material in Peking University Shenzhen Graduate School as a master under the supervision of Professor Feng Pan. His research interest focuses on the 3D printed front side metallization of silicon solar cells.

Zhou Gao received his B.S. degree in Chemistry from Peking University, China, in 2016. He is currently a master student in School of Advanced Materials, Peking University, China. His research is mainly focused on sliver paste for silicon solar cell.

Prof. Yuan Lin, Institute of Chemistry, Chinese Academy of Sciences (CAS), got B.S. from Dept. Chemistry, Peking University in1985, M.S and PhD from CAS in 1988 and 1995, respectively. In 1988-1999, he took the position of assistant professor at Institute of Photographic Chemistry, Chinese Academy of Sciences. From 1999 to present, he took the position of full professor. For more than 20 years, Prof. Lin has been engaged in the fields of photoelectrochemical conversion of solar energy, preparation of nanocrystalline semiconductors, investigation of photoelectrochemical and surface properties of nanocrystalline semiconductors, developing ionic liquid and polymeric materials for electrolytes.

Prof. Feng Pan, National 1000-plan Professor, Founding Dean of School of Advanced Materials, Peking University Shenzhen Graduate School, Director of National Center of Electric Vehicle Power Battery and Materials for International Research, got B.S. from Dept. Chemistry, Peking University in1985 and PhD from Dept. of P&A Chemistry, University of Strathclyde, Glasgow, UK, with "Patrick D. Ritchie Prize" for the best Ph.D. in 1994. With more than a decade experience in large international incorporations, Prof. Pan has been engaged in fundamental research and product development of novel optoelectronic and energy storage materials and devices. As Chief Scientist, Prof. Pan led 8 entities in Shenzhen to win the 150 million RMB grant for the national new energy vehicles (power battery) innovation project since 2013. As Chief Scientist, Prof. Pan led 12 entities to win National Key project of Material Genomic Engineering for Solid State Li-ion Battery in China in 2016.